Journal of Biomedical Optics 9(3), 648–654 (May/June 2004)

Optimization of selective hyperthermia

Christopher A. Bailey
Thomas M. Cowan
Vinson G. Liu
Evan C. Lemley
Wei R. Chen
University of Central Oklahoma
Department of Physics and Engineering
100 North University Drive, Edmond, Oklahoma 73034
E-mail: wchen@ucok.edu

Abstract. Selective hyperthermia can be a feasible treatment modality for deep tissue abnormalities. It is accomplished by using a laser or ultrasound noninvasively to transfer energy to a desired target causing tissue damage. This process has two potential benefits to medical professionals: simplicity of procedure and safety to patient. However, optimizing these selective interactions is difficult due to the number of variables. We propose an optimization coefficient relating the dynamic and geometric parameters of selective hyperthermia, and proceed to measure it in an experimental setup consisting of a near-infrared laser and laser-absorbing dye. To simulate tissue, gelatin phantoms are created using a combination of water, intralipid, and gelatin. Our experiments use a 1.00-cm-diam spherical phantom that is homogeneously enhanced with an indocyanine green (ICG) solution and placed inside a nontarget phantom and irradiated by an 805-nm diode laser. Temperature measurements taken at different locations are analyzed so optimization coefficients can be calculated for different parameters. This optimization coefficient compares the difference in temperatures from inside and outside the target. Analysis of the values after thermal equilibrium provides information about the best parameter selection. Our findings indicate that the optimal ICG concentration and power combination for our tested parameters are 0.083% and 0.97 W, respectively. Based on our analysis, optimization can be obtained by using this coefficient to compare the selectivity of several parameter combinations. [DOI: 10.1117/1.1689977]

Keywords: selective hyperthermia; optimization; near-infrared laser; indocyanine green.

03067 received May 20, 2003; revised manuscript received Sep. 3, 2003; accepted for publication Sep. 12, 2003.

1 Introduction

Tissue heating has been shown to be a way to destroy biological tissues. Cellular destruction of tumor tissue occurs[1] at or above a temperature of 42.5°C. It has also been observed that tumor tissue is more sensitive to temperature increases than normal tissue.[2] Therefore, it is possible to damage or kill tumor tissue, while keeping healthy tissue damage at a minimum, by using selective heating of the target tissue.

Selective hyperthermia can be achieved by transferring energy from external devices to a desired tissue region, which may be buried deep within nontarget tissue.[3,4] The possibility to induce the greatest selective effect by parameter selection increases the feasibility of selective hyperthermia for use in cancer treatment. A combination of an 805-nm diode laser, which has high tissue penetration capabilities, and an indocyanine green (ICG) solution, which has a strong absorption of light wavelengths around 800 nm, can be used in combination to achieve a selective effect.[5–8] The purpose for choosing this laser/dye combination is its use in laser immunotherapy.[9–13]

A major concern with selective hyperthermia in cancer treatment is its failure to destroy all of the cancer cells. Such failures could pose a problem when the surviving cancer cells proliferate after treatment. A method was devised to use selective hyperthermia to damage a local target tissue and at the same time induce a systemic response with the help of an immunoadjuvant.[9–13] To maximize the effectiveness of this procedure and minimize the possible side effects, the optimal parameter combination is desired. An optimization coefficient is necessary to rate the effectiveness of a treatment by comparing its selectivity. This value can be used to relate the variables of the experiment to the desired results. In the ideal case, the entire target region would be heated throughout by a homogeneous source with no heating to nondesired regions. In the actual case, heat diffusion out of the target region decreases the effectiveness of the treatment and lowers the selectivity. The goal, therefore, is to minimize the heating effect outside the target while maximizing the target heating. From this definition, a relationship can be derived that will provide a value to measure selectivity and determine optimal parameters.

2 Methods and Materials

2.1 *Absorption-Enhancing Dye*

ICG (Akorn, Buffalo Grove, Illinois) is the chemical that enables the selectivity of the laser light to occur. ICG has a high

Address all correspondence to Wei R. Chen, Ph.D., Associate Professor, Department of Physics and Engineering, University of Central Oklahoma, Edmond, Oklahoma 73034. Phone 405-974-5198. Fax: 405-974-3812.

1083-3668/2004/$15.00 © 2004 SPIE

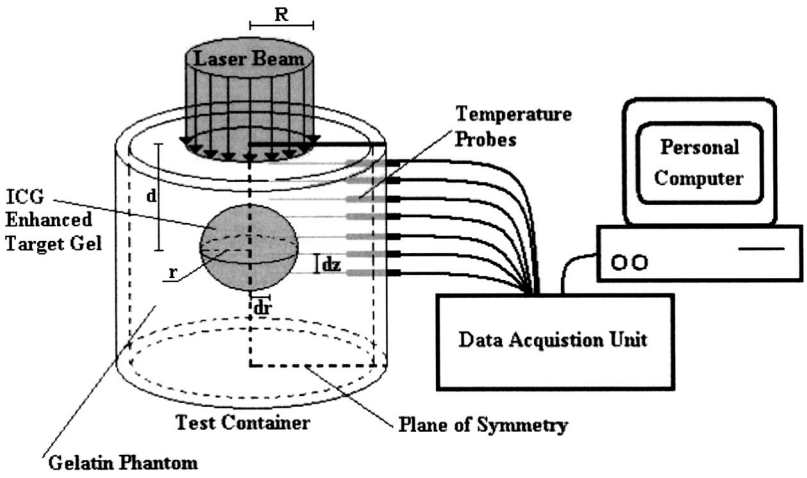

Fig. 1 Experimental setup of a gel phantom with an embedded ICG-enhanced target gel. The temperatures at specific locations were accessed by holes drilled into the side of the gelatin container. Temperature measurements were made by seven thermocouples attached to a computer via a data acquisition unit. Power was supplied to the gel region by an 805-nm diode laser centered along the axis of symmetry.

absorption peak around the 800-nm wavelength. It releases the absorbed energy in the form of heat to the surrounding tissue regions. To create selective hyperthermia, ICG must be inserted into the target region.

2.2 *Preparation of Gelatin Phantoms*

Gelatin phantoms were used in this experiment to simulate tissue structures with an embedded target region induced with laser-absorbing dye. Such gelatin phantoms have been used in preliminary experiments to create temperature distributions to find the existence of selectivity using gelatin targets and chicken breast tissue.[14] In this setup, however, the entire study was conducted with both target and nontarget regions being made of gelatin phantoms. The only difference between the two regions was the existence of ICG and slightly higher concentration of gelatin in the target phantom.

Nontarget phantoms were created by a combination of three materials: 80 mL water, 20 mL of Liposyn II 10% Intravenous Fat Emulsion (Abbott Laboratories, North Chicago, Illinois), and 2 g of gelatin (Leiner Davis Gelatin, Davenport, Iowa) per 100 mL of phantom solution. This solution was mixed and heated until the gelatin was melted, then solidified, and stored in a refrigerator. A cylinder of gelatin phantom 4.4 cm in diameter and 6.0 cm in depth was used to simulate a semi-infinite tissue region. Target phantoms were created in the same fashion as nontarget phantoms except for the use of 4 g of gelatin per 100 mL of solution. After the gelatin cooled to near room temperature, ICG solution was added to create the desired ICG concentration in the target phantom. This addition of ICG solution diluted the gelatin concentration to roughly that of the nontarget phantoms. A spherical target of 0.5 cm radius was used in our experiments. The ICG concentrations used in the target were: 0.000, 0.028, 0.056, 0.083, 0.111, and 0.139%.

2.3 *Gelatin Configuration for Experiment*

A container was created from clear acrylic tubing to minimize the optical interference of the tubing. A drill press with a 0.160-cm-diam drill bit was used to create the temperature probe holes on the wall of the container, which were used to hold the probes firmly into the container during laser irradiation. The spacing between the centers of the holes was 0.254 cm. The container was used to hold the gelatin during solidification and experimentation. To create two distinct regions of different optical properties, the gelatin was prepared in stages. First, the target gelatin was prepared and solidified in the desired shape (sphere) with a mold. Then the sphere was placed into the desired location and secured. Next, nontarget gelatin was prepared and poured into the container up to the middle of the target sphere and solidified. This ensured that we could visually see any shift in the targets location. Finally, the rest of the nontarget gelatin was poured into place and solidified.

2.4 *Laser and Optical Fiber*

The laser used in this experiment was the DIOMED 25 diode laser (DIOMEDICS, The Woodlands, Texas) with a wavelength of 805 nm. The laser beam was directed to the test site by an optical fiber with a diffusion lens (Pioneer Optics, Windsor Locks, Connecticut) to ensure an even distribution of laser energy on the treatment surface. The laser fiber was secured at a fixed position so that the beam radius would be a constant 1.0 cm throughout the experiments. The power output of the fiber was checked before each experiment and 0.35, 0.70, and 0.97 W were used.

2.5 *Temperature Measurements*

An Analog/Digital Signal Transducer Unit (InstruNet, GW Instruments, Somerville, Massachusetts) with multiple-channel temperature probes was used to measure phantom temperatures at specific locations during laser irradiation. Seven 27-guage T-series thermocouple probes (Omega Engineering, Stamford, Connecticut) were used in this experiment and placed at specific locations in the phantom container. Temperature measurements were taken every 2 s during laser irradiation, which lasted 750 s.

Twenty-eight probe locations were measured during this experiment. Seven probes were used to measure the temperatures at different depths, and were taken at four separate distances from the axis of symmetry. The radial distances of the probes from the axis of symmetry, shown in Fig. 1, were 0.00,

0.33, 0.66, and 1.00 cm. The depth probe positions from the surface were 0.254, 0.508, 0.762, 1.016, 1.270, 1.524, and 1.778 cm.

2.6 *Laser Irradiation of the Gelatin Phantom System*

The phantom was placed under the laser beam and the center of the laser was aligned with the center of the tumor. The gelatin phantom was allowed to come to room temperature, and then irradiated by the laser for 750 s. The temperatures at the probe tips were recorded during irradiation. Figure 1 provides a graphical representation of the experimental setup.

The 28 location temperature measurements were taken at seven positions at a time. Seven depth measurements at one radius were recorded in one treatment. Then the test region was allowed to return to a constant temperature and the probes were moved to the next location of different radius. This process was continued until all four radial positions temperatures were measured.

2.7 *Optimization Function*

To determine the optimum parameters, a function must exist that includes all the crucial physical parameters. Such an optimization value, referred to as η_s, is a function of time and the important parameters, which reflect geometry and physical properties. The setup geometry for this study can be narrowed to three properties, radius of the laser beam (R), depth of the tumor (d), and the radius of the tumor (r), as shown in Fig. 1. Likewise, the physical properties can be represented by two variable parameters: ICG concentration (I) and laser power (p). With these specific parameters chosen, η_s can be represented as

$$\eta_s = f(t,r,R,d,I,p). \tag{1}$$

Note that other important parameters do exist but they were held constant for our set of experiments.

Optimization, in general, must depend on the important parameters and the desired effect of the experiment. In our study, the desired effects of selectivity are

1. The heating effect in the nontarget region must be minimized.
2. The heating effect in the target region must be maximized.
3. The heating in the target must be as homogeneous as possible to cause the maximum amount of thermal damage.
4. The dosage of energy must cause a significant increase in the target's temperature.

To use these guidelines properly, ''critical'' regions must be defined in the medium. Critical regions are defined by how energy absorption affects the ability to heat the target. In our experiment, three major critical regions were defined as nontarget region R_0, heated target region R_1, and lesser-heated target region R_2, as shown in Fig. 2. Regions R_0, R_1, and R_2 were chosen because of their critical nature, and R_0 is the region where most of the surface energy is absorbed. Outside of R_0, the energy absorption from the laser drops off significantly. Also, R_1 is the region where a majority of the selective heat is absorbed, and R_2 is the lesser-heated target region where the major heating occurs from heat flow from other regions.

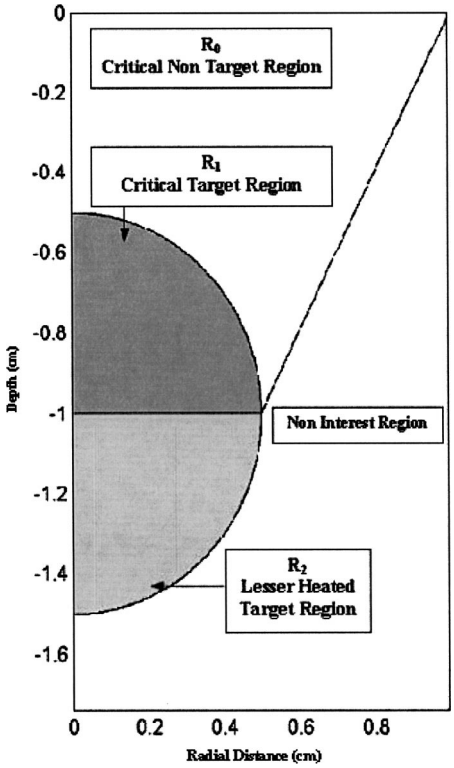

Fig. 2 Critical regions for our selective hyperthermia analysis. These regions were chosen to include the properties of beam and target radius and to enclose the majority of the absorbed laser energy. Here, R_0 is the region below the beam radius to the edge of the target sphere where most of the nontarget energy is absorbed; R_1 is the top half of the target, and is where a majority of the selective heat is absorbed; and R_2 is the bottom half of the target, and is where the major heating occurs mainly from diffusion.

Using these region definitions, the optimization coefficient η_S can be defined as

$$\eta_S = \frac{\overline{Q}_1 - \overline{Q}_0}{\overline{Q}_1 - \overline{Q}_2}, \tag{2}$$

where Q_0, Q_1, and Q_2 are the average energies absorbed by the laser in the regions R_0, R_1, and R_2, respectively. Note that this equation deals only with the energy absorbed directly from the source and not from diffusion of heat after absorption. When η_S is negative, selectivity does not occur. In the instance that η_S is zero, regions R_0 and R_1 are heated equally. If η_S is equal to ± 1, the average energy differences are distributed linearly or are very close to homogeneous. The goal of optimization will be to achieve the highest η_S value to ensure the greatest selective effect.

Energy absorption in tissue is difficult to measure experimentally. It is more convenient in theoretical or numerical simulations, but due to the experimental focus of this study it is used in a different form. In a real biological system, the tissue temperature rather than the absorption of energy di-

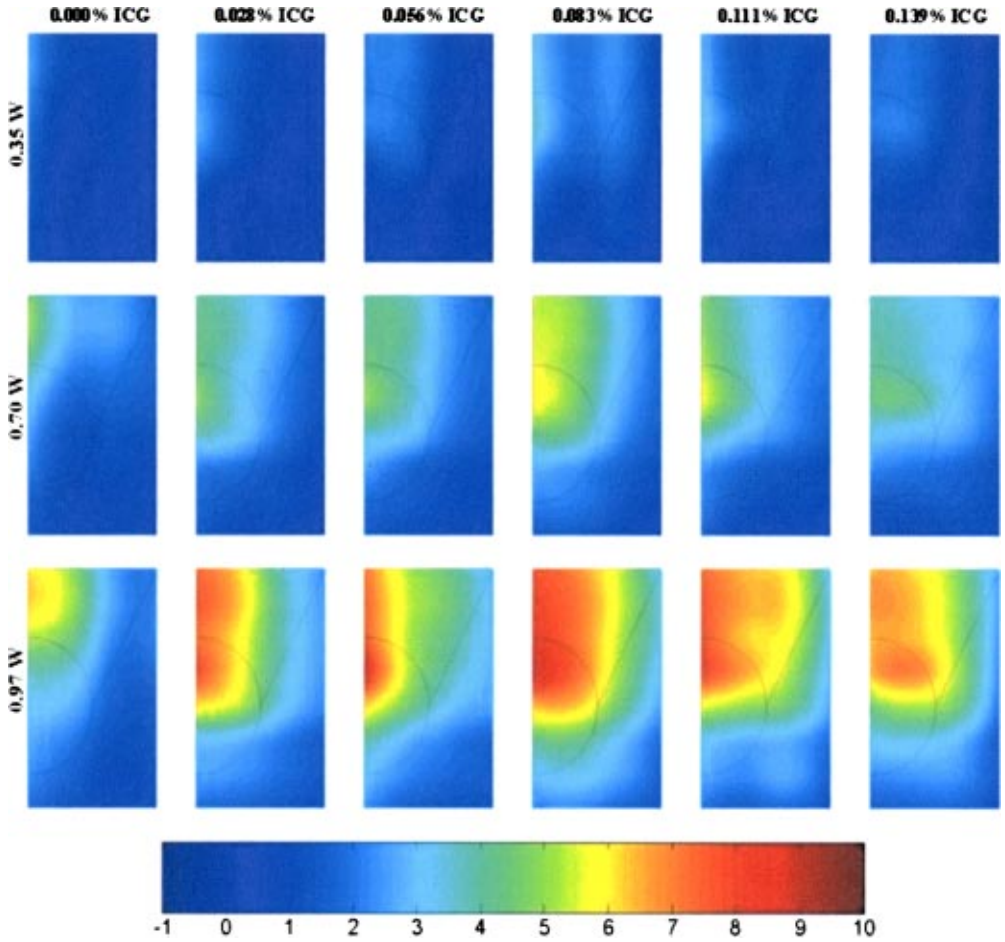

Fig. 3 False colors plots representing the temperature distributions in the phantom regions at 750 s, where the ICG concentrations vary from left to right and the laser powers from the top down. The target and nontarget critical regions are designated for orientation purposes, and the spatial scale is the same as that in Fig. 2. The color designation represents temperature changes in the medium from −1 to 10°C.

rectly determines the outcome of the cancer treatment. Therefore, temperature changes are more beneficial to our purpose, so we adjust Eq. (2) to arrive at

$$\eta_{\mathrm{ST}}=\frac{\overline{T}_1-\overline{T}_0}{\overline{T}_1-\overline{T}_2}, \tag{3}$$

where η_{ST} is the selective thermal optimization coefficient; and T_0, T_1, and T_2 are the average temperatures in regions R_0, R_1, and R_2 respectively.

2.8 *Data Fitting of Temperature Measurements*

Polynomials were used to approximate the temperature changes versus time, and the best-fit equation is

$$\Delta T=\alpha t^6+\beta t^5+\chi t^4+\delta t^3+\varepsilon t^2+\phi t+\varphi. \tag{4}$$

The coefficients in Eq. (4) were organized and transferred into matrix form. Converting the data in this fashion allowed us to compress the 375 temperature measurements at a particular position into seven coefficients calculated by the best-fit using Eq. (4). The coefficients from Eq. (4) were organized by inserting them into matrix **M**:

$$\mathbf{M}(I,p,r_p,d_p,:)=[\alpha,\beta,\chi,\delta,\varepsilon,\phi,\varphi]. \tag{5}$$

The indices of matrix **M** represent all the parameters used in the organization of the coefficients mentioned in Eq. (4). Index I represents the six ICG concentrations that were used in the experiment. Index p represents the three power levels that were used. The indices r_p and d_p represent the probe location in the medium.

2.9 *Finite Element Integration*

To meet the definition of optimization determined in Eq. (3), the average temperature change in the critical regions must be calculated. Finite element calculations were used in the form

$$\Delta\mathbf{T}_{\mathrm{ave}}=\frac{\Sigma_{i=1}^{m}\Sigma_{j=1}^{n}\mathbf{T}(t)_{ij}\Delta V_{R_{ij}}}{V_R}. \tag{6}$$

The **T** matrix is the temperature distribution in the region, examples of which can be seen in the false color plots of Fig. 3. The spatial matrix element $\mathbf{T}_{ij}$ calculated at time t, is weighted by the finite volume element $\Delta V_{R_{ij}}$. The volume element is a cylindrical ring created by the size of the spatial element in $\mathbf{T}_{ij}$ about the axis of symmetry. The result is a

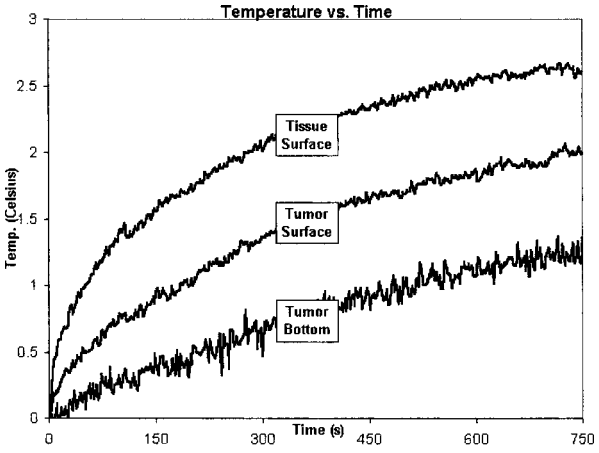

Fig. 4 Temperature measurements taken at the $r = 0.000$ cm location, along the axis of symmetry, for a power of 0.35 W and 0.000% ICG. The temperature change decreases in magnitude as the depth of the probe increases. This is the definition of a nonselective situation.

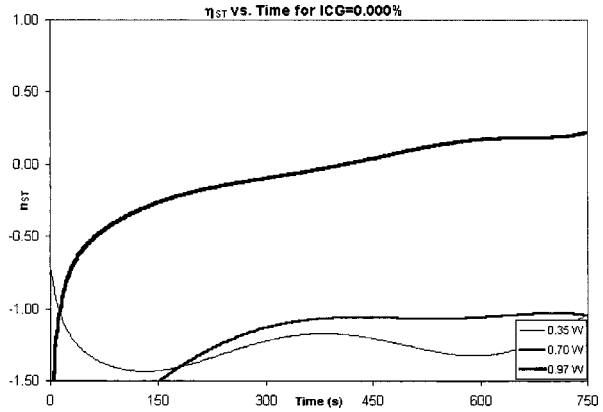

Fig. 6 Plots of η_{ST} [Eq. (3)] versus time for the three powers and 0.000% ICG target concentration. Notice the negative values in this situation, which indicates their nonselective nature. The 0.97-W value does seem to move into the selective region, however, if compared to the plots of these in Figs. 7 and 8 the 0.97-W plot value is still too low to be considered optimum.

finite-element average of temperature changes in the desired region. These average values were inserted into Eq. (3) to give the optimization coefficient at a measured time *t*.

3 Results

3.1 *Temperature Distributions in Gelatin Phantom*

Temperatures at different locations in the gelatin system were measured during laser irradiation. Figures 4 and 5 provide examples of these temperature differences versus time with and without an ICG enhanced target. Temperature change rather than absolute temperature was used because the regions were very close to homogeneous when the data was initialized. The differences between Figs. 4 and 5 occur in the relative locations of the tissue surface and tumor surface temperature values. Figure 4 shows no signs of selectivity, because the temperature decreased as the depth increased. Figure 5, however, shows the desired selectivity because the temperature at the tumor surface is higher than that at the tissue surface.

3.2 *Optimization Coefficients*

Average temperatures were calculated for each critical region using Eq. (6). The optimization coefficient for each time measurement was determined by Equation (3). The resulting optimization curves can be seen in Figs. 6 through 8. Figure 6 shows a case of no selectivity because of the negative values of η_{ST}, while Figs. 7 and 8 do represent selectivity with the existence of positive values.

3.3 *Thermal Equilibrium Optimization*

In each of the experiments, the optimization curves fluctuate about a constant value after 100 s. After which, an average and standard deviation of the optimization values were calcu-

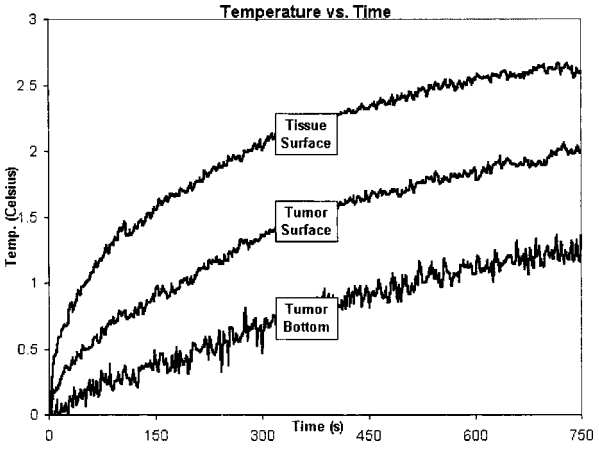

Fig. 5 Temperature measurements taken in the same location and power as those in Fig. 4, but with an ICG concentration of 0.139%. The temperature measurements in this case differ from those in Fig. 4 in that the tumor measurement is higher than the surface measurement. This presents evidence of selectivity.

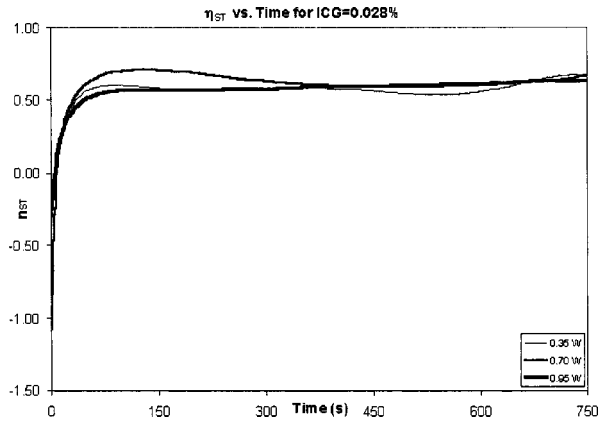

Fig. 7 Plots of η_{ST} versus time for each power and an ICG concentration of 0.028%. In this case, the selectivity for each power level is almost constant, and they all approach their critical value after about 100 s. This is when the transient part of the heat transfer is considered to be at an end and the stability of selectivity is achieved.

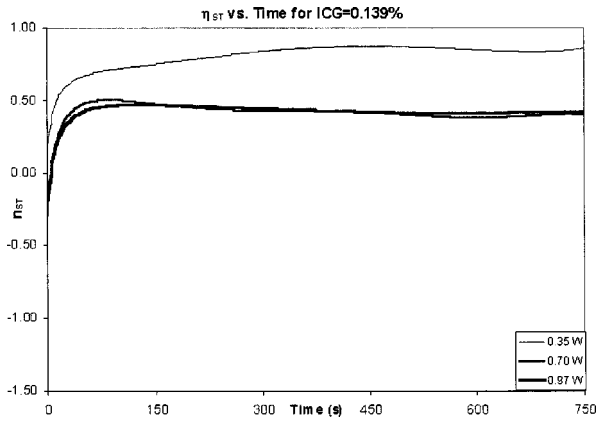

Fig. 8 Plots of η_{ST} versus time for 0.139% ICG gel concentration. In this case, the barrier effect is too large for our power levels to overcome. This plot is the reverse case of that shown in Fig. 7, because the ICG concentration is too high for our powers to be effective.

lated. To calculate the optimized parameters for different combinations, the thermal equilibrium optimization coefficient and the average steady state temperature value for region 1 were used. Both values are required because the optimization coefficient of Eq. (3) provides information on the selective nature of the treatment, and the average temperature helps to estimate the dosage applied. When combined these two values help to satisfy the criteria of selectivity stated in Sec. 2.7.

3.4 *Optimized Parameters*

The optimum parameters were chosen to create the maximum temperature increase in the target while maximizing the selectivity of the treatment. These properties are indicated by the weighted optimization coefficient, which is the multiplication of the optimization coefficient and the average steady state temperature in region 1, listed in Table 1, which show that the optimal parameter combination for our tissue phantoms is 0.083% and 0.97 W with a value of 4.06±0.07°C. From the data provided in Table 1, a trend occurs for the weighted η_{ST} value, which is directed from low power/high concentration to high power/low concentration and can been seen by the cells in the table which are in bold fonts. This indicates that a relationship can possibly be determined with further investigation.

Table 1 Table of weighted η_{ST} values after 100 s with standard deviations for different power and ICG concentration combinations.

ICG	0.35 W	0.70 W	0.97 W
0.000%	−0.75±0.04°C	−2.03±0.21°C	0.03±0.40°C
0.028%	0.84±0.03°C	2.16±0.07°C	**3.51±0.12°C**
0.056%	1.26±0.11°C	2.09±0.04°C	2.17±0.05°C
0.083%	0.23±0.14°C	**2.89±0.09°C**	**4.06±0.07°C**
0.111%	0.72±0.05°C	2.08±0.04°C	1.19±0.13°C
0.139%	**1.48±0.05°C**	1.58±0.08°C	2.70±0.06°C

4 Discussion

The objective of the study reported here was to devise a systematic approach to find optimum parameters in selective hyperthermia. This was accomplished by defining a value that depended on the important parameters. Temperature measurements were taken in the gelatin phantom irradiated by the laser. Finite-element integration was used to average the temperature distributions so the optimization coefficients could be calculated for each parameter combination. Using an ICG-enhanced target gelatin embedded inside regular nontarget gelatin, selectivity was demonstrated by the temperature distributions, as shown in Figs. 4 and 5. Careful temperature, position, and time measurements were made to determine the temperature distributions within the test regions. The correct target/nontarget configuration is obtained by securing the solidified gelatin tumor in the desired location prior to pouring the nontarget gelatin. Critical regions were chosen to encapsulate a majority of the transmitted energy, and were based on Monte Carlo simulations of these selective cases, which calculated the regions where absorbed energy could be contained.[15,16] The optimization coefficient definition included the predefined critical regions and the considerations of energy absorption in those regions, which leads to Eq. (2). The relationship between the temperature and energy can be shown by the heat equation:

$$\rho C_p \frac{\partial T}{\partial t} = k\nabla^2 T + \dot{q}, \tag{7}$$

where T is the temperature at any position in the region, ρ is the material's density, C_p is the heat capacity, k is the thermal conductivity, and $\dot{q}$ is the power density distribution within the material. When enough time has elapsed, the temperature at any location will become constant. The steady state version of the heat equation inherently provides a constant η_{ST}, as shown in Figs. 6 to 8, and must obey the constraint $|\eta_{ST}| \leqslant |\eta_S|$ because of heat diffusion in the material.

Note that the use of Eqs. (2) and (3) has some limitations. Two possible scenarios can occur such that an undefined optimization value could be obtained. One is when the target receives no energy at all (i.e., no temperature change). The second situation is if the average energies or temperatures in the two critical target regions are equal. The following explains the limitations of the optimization coefficients, and why the undefined situations should not arise in our inspection of the optimization coefficients.

1. The optimization values are valid only while heating is occurring. Therefore, any situation where no energy is being transferred is considered an invalid use of the optimization equations.
2. The reason to use such optimization values is to evaluate the effectiveness of a selective heating treatment,

and geometries such as ''infinitely deep'' tissues would be an ineffective configuration for laser treatment, and should not be studied in this manner.

Plots of the optimization coefficients versus time showed a tendency of the optimization coefficient to approach a constant value after approximately 100 s. The optimization values, given in Table 1, were averaged after 100 s, so that an optimized parameter set could be chosen. The plots in Fig. 6 of η_{ST} versus time for the control (0.000% ICG) illustrate nonselective behavior in all three powers. The 0.97-W plot seems to deviate into the selective range. This is possibly due to the relatively higher power and temperature and the slightly denser gelatin concentration, which enabled the energy to be distributed quicker in the target region, increasing the selectivity of the control. It was not significant at the lower powers because there was not enough energy for this structural difference to be observed. The value of η_{ST} eventually stabilized, which is consistent with the experiments when ICG is present. Figure 7, unlike Fig. 6, shows a situation that is highly structured and selective. It appears that the introduction of ICG creates consistency in the optimization coefficient. The optimization value approaches this critical value very quickly and then stabilizes, separating the transient and equilibrium time increments. In Fig. 8, the transition seems to follow the same process as that of Fig. 6, but in reverse. Although the target gelatin in Fig. 6 contained no ICG, Fig. 8 has too much ICG, creating a laser-absorbing barrier that cannot be overcome by the power levels used in our experiments. The average values and standard deviations of the weighted form of η_{ST} for each of the parameter sets are charted in Table 1. This enables us to view the average value of the weighted optimization coefficient for a particular parameter set and compare it to those of other combinations.

The method of using the optimization value η_{ST} as proposed in our study could be used as guidance for clinical applications of selective hyperthermia using laser, ultrasound, or other treatment modalities. Future investigations using theoretical simulations, *in vitro*, and *in vivo* experiments will further provide valuable information on the optimization of the dye-enhanced selective hyperthermia, paving the way for clinical applications.

Acknowledgments

This research was supported in part by grants from the Dr. Joe C. Jackson College of Graduate Studies & Research, the University of Central Oklahoma, and from the Oklahoma Center for the Advancement of Science & Technology (OCAST) No. AP00(2)-011P and AP01-016.

References

1. W. C. Dewey, L. E. Hopwood, S. A. Sapareto, and L. E. Gerweck, ''Cellular responses to combinations of hyperthermia and radiation,'' *Radiology* **123**, 463–474 (1977).
2. L. J. Anghileri and J. Robert, *Hyperthermia in Cancer Treatment*, CRC Press, Boca Raton, FL (1986).
3. H. H. Leveen, S. Wapnick, V. Riccone, G. Falk, and N. Ahmed, ''Tumor eradication by radio frequency therapy,'' *J. Am. Med. Assoc.* **235**, 2198–2200 (1976).
4. J. B. Marmor, D. Pounds, D. B. Postic, and G. M. Hahn, ''Treatment of superficial human neoplasms by local hyperthermia induced by ultrasound,'' *Cancer* **43**, 196–205 (1979).
5. W. R. Chen, R. L. Adams, S. Heaton, D. T. Dickey, K. E. Bartels, and R. E. Nordquist, ''Chromophore-enhanced laser-tumor tissue photothermal interaction using an 808-nm diode laser,'' *Cancer Lett.* **88**, 15–19 (1995).
6. W. R. Chen, R. L. Adams, K. E. Bartels, and R. E. Nordquist, ''Chromophore-enhanced in vivo tumor cell destruction using an 808-nm diode laser,'' *Cancer Lett.* **94**, 125–131 (1995).
7. M. D. Lucroy, W. R. Chen, D. Sensney-Spears, R. G. Higbee, and K. E. Bartels, ''Improved light delivery for chromophore-enhanced laser-induced hyperthermia in a subcutaneous murine breast cancer model,'' *Proc. SPIE* **4244**, 561–566 (2001).
8. M. D. Lucroy, W. R. Chen, T. D. Ridgway, R. G. Higbee, and K. E. Bartels, ''Selective laser-induced hyperthermia for the treatment of spontaneous tumors in dogs,'' *X-Ray Sci. Technol.* **10**, 237–243 (2002).
9. W. R. Chen, R. L. Adams, R. Carubelli, and R. E. Nordquist, ''Laser-photosensitizer assisted immunotherapy: a novel modality for cancer treatment,'' *Cancer Lett.* **115**, 25–30 (1997).
10. W. R. Chen, W.-G. Zhu, J. R. Dynlacht, H. Liu, and R. E. Nordquist, ''Long-term tumor resistance induced by laser photoimmunotherapy,'' *Int. J. Cancer* **81**, 808–812 (1999).
11. W. R. Chen, H. Liu, J. A. Nordquist, and R. E. Nordquist, ''Tumor cell damage and leukocyte infiltration after laser immunotherapy treatment,'' *Lasers Med. Sci.* **15**, 43–48 (2000).
12. W. R. Chen, A. K. Singhal, H. Liu, and R. E. Nordquist, ''Laser immunotherapy induced antitumor immunity and its adoptive transfer,'' *Cancer Res.* **61**, 459–461 (2001).
13. W. R. Chen, J. W. Ritchey, K. E. Bartels, H. Liu, and R. E. Nordquist, ''Effects of different components of laser immunotherapy in treatment of metastatic tumors in rats,'' *Cancer Res.* **62**, 4295–4299 (2002).
14. V. G. Liu, T. M. Cowan, S.-W. Jeong, S. L. Jacques, E. C. Lemley, and W. R. Chen, ''Selective photothermal interaction using an 805-nm diode laser and indocyanine green in gel phantom and chicken breast tissue,'' *Lasers Med. Sci.* **17**(4), 272–279 (2002).
15. L.-H. Wang, R. E. Nordquist, and W. R. Chen, ''Optimal beam size for light delivery to absorption-enhanced tumors buried in biological tissues and effect of multiple beam delivery: a Monte Carlo study,'' *Appl. Opt.* **36**, 8286–8291 (1997).
16. L.-H. Wang, G. Marquez, R. E. Nordquist, and W. R. Chen, ''Propagation and absorption of near-infrared laser light in photosensitizer-enhanced biological tissues,'' *Proc. SPIE* **3254**, 332–339 (1998).